Wu *et al. Advanced Modeling and Simulation in Engineering Sciences(2022)9:14*
https://doi.org/10.1186/s40323-022-00228-6

Advanced Modeling and Simulation in Engineering Sciences

RESEARCH ARTICLE Open Access

Numerical modeling of the propagation process of landslide surge using physics-informed deep learning

Yinghan Wu[1], Kaixuan Shao[1], Francesco Piccialli[2] and Gang Mei[1*]

*Correspondence: gang.mei@cugb.edu.cn
[1]School of Engineering and Technology, China University of Geosciences (Beijing), Beijing, China
[2]Department of Mathematics and Applications, University of Naples Federico II, Naples, Italy

Abstract

The landslide surge is a common secondary disaster of reservoir bank landslides, which can cause more serious damage than the landslide itself in many cases. With the development of large-scale scientific and engineering computing, many new techniques have been applied to the study of hydrodynamic problems to make up for the shortcomings of traditional methods. In this paper, we use the physics-informed neural network (PINN) to simulate the propagation process of surges caused by landslides. We study different characteristics of landslide surges by changing water depth and particle density. We find that: (1) the landslide surge propagation process simulation method based on the physics-informed neural network has good applicability, and the stages of landslide surge propagation can be well presented; (2) the depth of water influences the landslide surge propagation as the amplitude of the surge increases with deeper water; (3) the particle density of water influences the landslide surge propagation as the fluctuation of the surge is more obvious with larger particle density. Our study is helpful to understand the propagation process of landslide surges more clearly and provides new ideas for the follow-up study of this kind of complex fluid–structure interaction problem.

Keywords: Geological hazards, Landslide surge, Deep learning, Physics-informed neural network (PINN)

Introduction

The landslide surge is a secondary geological disaster. It is caused by a partial or entire slope rapidly impacting certain water after the slope is unstable and destroyed [1], which causes great damage to the surrounding environment and the safety of human life and property [2]. There have been a lot of landslide surge disasters in history. In 1958, the maximum surge generated by the landslide in Lituya Bay, Alaska, reached 524 m high and made it the highest record in history [3,4]. In 1963, the Vajont reservoir in Italy was destroyed. A mass of nearly 300 million m^3 of rock and debris fell into the reservoir and generated a wave that over-topped the 261.6 m high dam built across the gorge [5]. Approximately 2000 people were killed in the disaster [6]. In addition to the landslide surges that have occurred in history, many potential landslides may cause serious hazards. The unstable

slides of the landslide Åkneset in western Norway continue to move at a rate of 15 cm per year [7]. Effective landslide surge disaster prediction research is very important.

At present, the research on the landslide surge mainly covers three aspects: theoretical analysis [8], physical experiment [9], and numerical simulation [10]. Theoretical derivation methods usually simplify real conditions based on assumed models. Mulligan et al. [11] derived the analytical solution of the maximum height of the surges in the near field according to the momentum conservation of the landslide and water. Physical experiments and numerical simulations are generally used for complex practical problems such as boundary conditions. The preliminary physical experiments are mainly based on two-dimensional or semi-infinite space conditions. However, Heller et al. [12] pointed out that surges in two-dimensional conditions were overestimated and three-dimensional surges attenuated faster. In the later stage, a series of 3D simulation experiments were carried out. Panizzo et al. [13] derived the correlation index from the three-dimensional experiment, which can be well applied to the actual surges in the Vajont reservoir.

Although physical experiments are of high reliability, the cost is high and the relevant physical information is difficult to obtain comprehensively [14]. Compared with physical tests, numerical simulation is more flexible and convenient to consider the effect of geological structure and water conditions on landslide surges in actual situations. At present, most of the numerical simulation methods of landslides are to simulate the movement of the discontinuous medium. Mainly including the Discrete Element Method (DEM) [14], the Discontinuous Deformation Analysis (DDA) [15], and the Numerical Manifold Method (NMM) [16], etc., but these methods can not directly simulate the surges generated later. Considering the different mechanical properties of blocks and fluids, some scholars have coupled the Computational Fluid Dynamics (CFD) and discontinuous numerical methods [17], such as the coupled CFD-DEM Approach [18] and the hybrid DEM-SPH Model [19], etc. When solving partial differential equations (PDE), numerical methods such as the Finite Difference Method (FDM) [20] and the Finite Element Method (FEM) [21] are mostly adopted. Most of these numerical methods need to be discretized when solving complex PDEs. This method directly correlates between the efficiency and accuracy of the calculation and the mesh density and the calculation step size, greatly limiting the solving process and results.

The physics-informed neural network (PINN) was proposed by Raissi et al. [22]. It embeds PDEs such as principles of physical laws or other professional knowledge into neural networks to achieve accurate solutions for different types of PDEs by constraining the loss function. The rationality of the obtained solution is limited by embedding physical information, which helps the algorithm to perform better learning optimization in the case of a small number of training samples. Besides, the calculation accuracy is independent of the calculation step size, so PINNs are expected to solve problems in traditional numerical methods, such as dimensional disasters, inverse problem solving, etc. At present, the application research of PINNs has made great progress in many fields. Kissas et al. [23] used PINN to determine unknown flow variables in a given arterial network and applied it to real clinical cases. Mao et al. [24] studied the possibility of using PINN to approximate the Euler equation of high-speed aerodynamic flow. Jin et al. [25] employed PINNs to solve some problems in incompressible Navier–Stokes equations.

In this paper, we preliminarily study the propagation of landslide surges using PINN. We simulate the surge propagation caused by a block falling into the water. We first construct

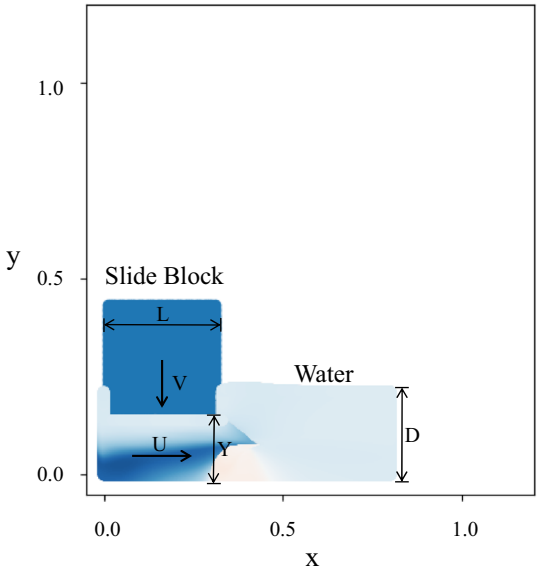

Fig. 1 Schematic diagram of the landslide surge model

a rigid landslide surge model based on PINN. On this basis, we draw the morphological characteristics of the surge at different times and analyze the propagation process of the surge. Then we study the influence of the depth and particle density of water on the propagation respectively by controlling variables.

The rest of this paper is organized as follows. "Materials and methods" section will briefly introduce a rigid landslide surge model based on PINN and related theories. "Results and analysis" section will present the simulation results of the surge propagation process under different conditions and analyzes the influence of water depth and particle density. "Discussion" section will discuss the applicability of PINN to the study of this type of problem and other methods that may be applicable. Finally, several conclusions will be drawn in "Conclusions" section.

Materials and methods

Simple landslide surge model

In this paper, we construct the following model concerning the classic Scott Russell's wave [26] as a simple simulation of rigid landslide surges. As shown in Fig. 1, we use a slide block with an initial velocity of 0 to fall into the water to simulate the process of surges caused by a rigid landslide falling into the water after it becomes unstable in a static state. We define the mass of the slide block as M, the length as L, and the width of the slide block and water tank as W. When the slide block is in the initial position, its bottom height Y from the bottom of the water tank is the same as the depth D of water.

Mathematical model used to describe the landslide surge

Conservation laws in fluid mechanics

The water in this study is regarded as two-dimensional inviscid incompressible fluid, which conforms to Euler equations of conservation laws in fluid mechanics. Conservation laws mainly include the conservation of mass, momentum, and energy.

The conservation of mass:

$$\frac{\partial u}{\partial x}+\frac{\partial v}{\partial y}=0 \tag{1}$$

The conservation of momentum:

$$\begin{aligned}&\frac{\partial u}{\partial t}+u\frac{\partial u}{\partial x}+v\frac{\partial u}{\partial y}=f_x-\frac{\partial p}{\rho\partial x}\\&\frac{\partial v}{\partial t}+u\frac{\partial v}{\partial x}+v\frac{\partial v}{\partial y}=f_y-\frac{\partial p}{\rho\partial y}\end{aligned} \tag{2}$$

In Eqs. (1) and (2), u and v are the components of the velocity in the direction of x and y, p is the pressure, and f is the external force exerted on the fluid per unit volume.

According to the above description of basic parameters and the derivation of slide block velocity, we build a basic model to simulate the landslide surges combined with the governing equation of inviscid incompressible fluid movement laws.

Empirical equations

Fluid–structure interaction knowledge is needed to study how the slide block interacts with the water. In this study, we mainly use empirical equations to describe this process. According to the study of Monaghan et al. [27], the water below the slide block can be approximated as horizontal motion during the falling process. We define the vertical falling velocity of the slide block at a certain moment as V, the horizontal velocity of the water under the slide block as U, and the distance between the bottom surface of the slide block and the bottom of the water tank as Y.

According to the conservation of mass, the vertical falling velocity V and the horizontal velocity U relate as:

$$V=UY/L \tag{3}$$

The vertical velocity V of the slide block is:

$$\frac{V}{\sqrt{gD}}=\frac{Y}{D}\left(1-\frac{Y}{D}\right)^{1/2}\left(\frac{D}{L}\right)^{(2-\beta)/2}\left(\frac{M}{\rho LDW}\right)^{1/2} \tag{4}$$

where β is arbitrary. In this study, we take β to be 1.

Modeling of landslide surge propagation using PINN

The PINN learns by minimizing the sum of the squared errors. The sum square error equation of the neural network model is described as:

$$\mathcal{L}=MSE_{\mathbf{v}}+MSE_{\mathrm{div}\,\mathbf{v}}+MSE_{\mathbf{p}} \tag{5}$$

$$MSE_{\mathbf{v}}=\frac{1}{N}\sum_{i=1}^{N}\left|\mathbf{v}^{i+1}-\mathbf{v}^{i}\right|^2 \tag{6}$$

$$MSE_{\mathrm{div}\,\mathbf{v}}=\frac{1}{N}\sum_{i=1}^{N}\left|\mathrm{div}\,\mathbf{v}^{i}\right|^2 \tag{7}$$

$$MSE_{\mathbf{p}}=\frac{1}{N}\sum_{i=1}^{N}\left|\mathbf{p}^{i+1}-\mathbf{p}^{i}\right|^2 \tag{8}$$

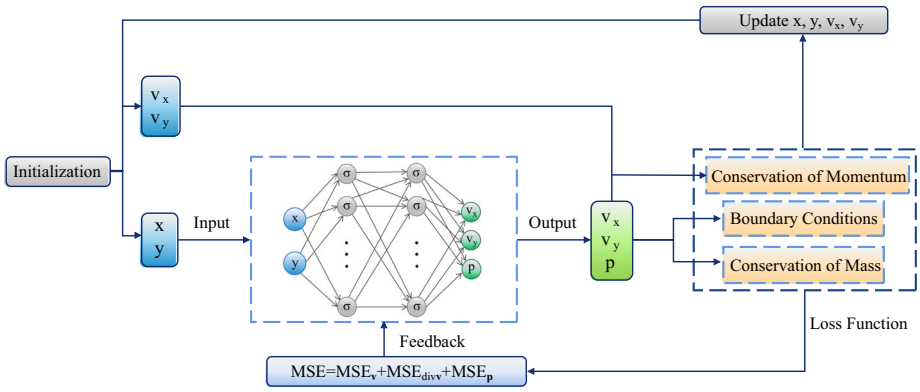

Fig. 2 Schematic of the PINN for the simulation of the landslide surge propagation process

$MSE_{\mathbf{v}}$ is the error between the velocity predicted by the neural network and the value controlled by the conservation of momentum. The conservation of mass is controlled by the square sum of the divergence of the velocity predicted by the neural network, as shown in Eq. (7). $MSE_{\mathbf{p}}$ is the square sum of the error between the boundary pressure predicted by the neural network and the boundary pressure derived from Dirichlet boundary conditions.

Dirichlet boundary is adopted as the boundary of the model, the water surface is regarded as the free boundary, and the pressure at the boundary is zero. The side wall and bottom wall are regarded as fixed boundaries, and the velocity perpendicular to the boundary is zero. The initial condition is the static state when the bottom surface of the block is not in contact with the water.

We use a fully connected neural network of 2 input neurons, 2 hidden layers with 60 neurons each, and 62 output neurons. The spatial coordinates (x, y) are fed into the neural network as input, where this model predicts the velocity and pressure as the output. A subset of liquid particles is used for training. We apply the tanh function as the activation function in the neural network. The L-BFGS-B optimizer provided by the SciPy package [28] is chosen to train 12,000 epochs for this experiment.

In this paper, PINN is used to simulate the landslide surge propagation process as follows. First, the position information $\mathbf{x}$ and $\mathbf{y}$ of the initialized fluid particles are input into the fully connected neural network by predicting the output velocities $\mathbf{v}_x$ and $\mathbf{v}_y$ in the two directions. Then, the loss function is constructed based on the conservation of mass, the conservation of momentum, and boundary conditions. Finally, after continuous feedback adjustment to minimize the loss, the position and velocity of fluid particles are updated and input into the next time step. The flowchart of the PINN for the propagation process of landslide surge is given in Fig. 2.

We illustrate the method for preliminarily studying the propagation of landslide surges with PINN by using a working flow chart, as shown in Fig. 3. We simulate the surge propagation caused by a slide block falling into the water. We first construct a landslide surge model based on PINN. On this basis, we draw the morphological characteristics of the surge at different times and analyze the propagation process of the surge. Then we study the influence of the depth and particle density of the water on the propagation respectively by controlling variables.

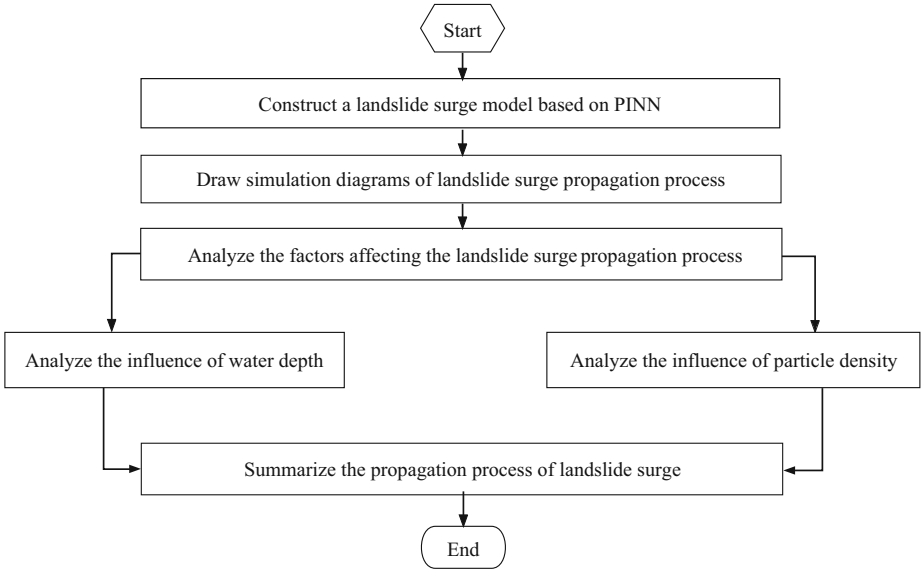

Fig. 3 Flow chart of the method for simulation of the landslide surge propagation process

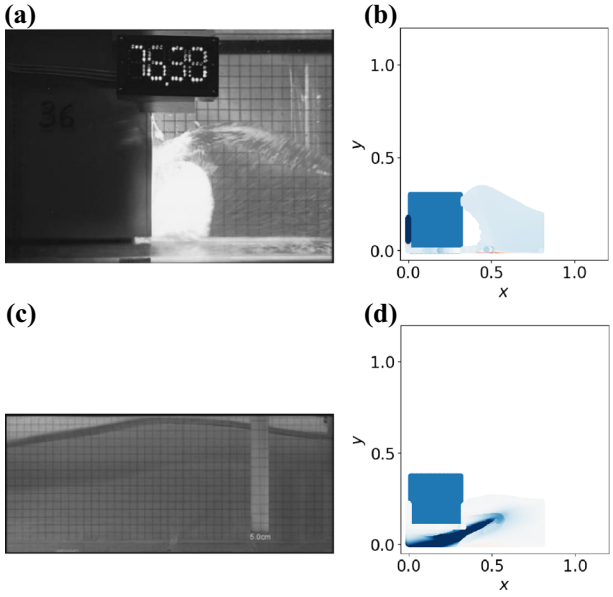

Fig. 4 Comparison between simulation results of landslide surge propagation process based on PINN and physical experiment results [27] (D = 0.21 m, n = 200/m)

Results and analysis

We use the PINN to simulate the propagation process of the surges after the slide block falls into the water. We analyze the surge shape and height in the simulation. At the same time, we analyze the influence of the initial depth and particle density of water on the characteristics of the surges. In this paper, other basic parameters besides water depth and particle density are set as follows. The length of the water tank is 800 mm, the length of the block is 300 mm, the width of both the water tank and the block is 400 mm, the density of the water is 1000 kg/m^3, the gravitational acceleration is -9.8 m/s^2,

the collision recovery coefficient is 0.25, the Poisson's ratio of the block is 0.3, and the permeability coefficient is 0.01. Time step $dt = 0.01$ s.

Reliability analysis

Compared with the physical experiment in related literature, the simulation results are consistent with the physical experiment results, indicating that this study is reasonable and valid. Figure 4 shows the comparison between simulation results of landslide surge propagation process based on PINN and physical experiment results [27] (D = 0.21 m, n = 200/m).

Simulation and analysis of the surge propagation process

Simulation and analysis of the surge morphology and pressure distribution

First, we choose water depth $D = 0.21$ m and particle density $n = 200/\text{m}$ as examples to analyze the propagation process of the surge. Under such conditions, the morphology and pressure changes of the surge at different times are shown in Fig. 5. At the initial contact with water, the surface of the water does not change significantly. Part of the water in contact with the block depresses slightly, and there is an area of significantly increased pressure in the deeper part of the water on the lower right of the block. As the block

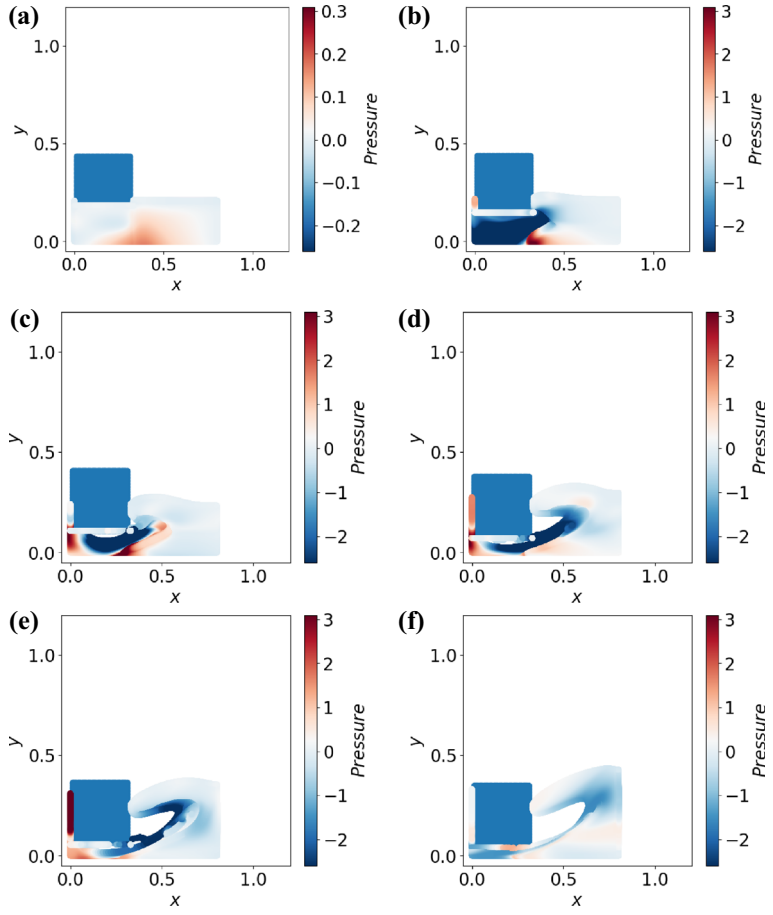

Fig. 5 The surge morphology and pressure distribution diagram. Water depth $D = 0.21$ m and particle density $n = 200/\text{m}$. Each map corresponds to a different moment. **a** 2 dt. **b** 4 dt. **c** 6 dt. **d** 8 dt. **e** 9 dt. **f** 10 dt

continues moving downward, part of the water beneath it is pushed to the right with the impact. The water next to the right of the block is lifted by compression. The surge begins to form gradually. Then, as more water is pushed to the right, the height of the wave gradually increases. At the same time, a small part of water enters the gap between the left side of the block and the wall with extrusion. The water on both sides of the bottom of the block is compressed and the pressure increases obviously. After that, the water on the right side overturns with the continuous impact of the water at the bottom of the block, forming a tip downward surge in the opposite direction of propagation. At this time, the internal cavity of the overturned water formed. Under the action of extrusion and impact, the height of the wave on the right side of the block increases continuously. The water in the gap on the left side of the block also rises until it exceeds the top of the block.

Simulation and analysis of the surge flow and divergence

In order to have a clearer understanding of how water flows during surge formation, we study the divergence of the water during the block falling into the water. Divergence describes the volume density of flux and the magnitude of velocity concentration and dispersion. Divergence greater than 0 means there is a net outflow of fluid. Divergence at different times when water depth $D = 0.21$ m is shown in Fig. 6. When the block just enters the water, the fluid beneath the block moves to the right under compression. As the block continues downward, most of the water to its right is lifted by the impact. At the same time, a small amount of water enters the gap between the slide block and the left wall and continues rising, which is consistent with the previous analysis based on the

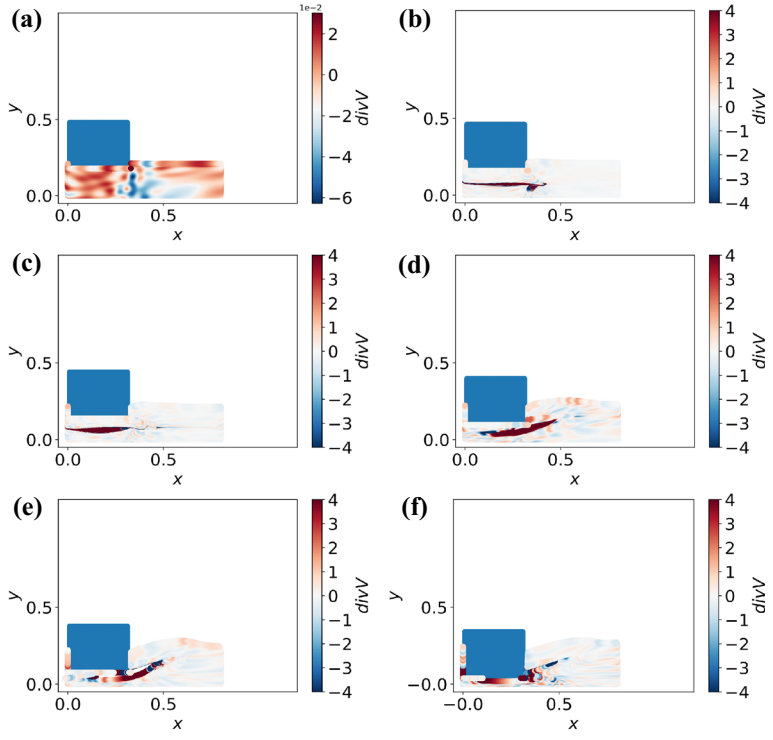

Fig. 6 The surge morphology and divergence distribution diagram. Water depth $D = 0.21$ m. Each map corresponds to a different moment. **a** 2 dt. **b** 3 dt. **c** 4 dt. **d** 6 dt. **e** 7 dt. **f** 9 dt

wave morphology and pressure. By drawing the divergence distribution diagram, we can understand the flow of water in each part during the formation of the surge more clearly and concretely.

Influence of water depth on characteristics of the surge

Simulation results when water depth D = 0.116 m

The depth of the water may affect the formation and propagation of the landslide surges. To study this effect, we only change the water depth for further analysis. Figure 7 shows morphology and pressure changes of the surge at different times when water depth $D = 0.116$ m and particle density $n = 200/\text{m}$. When the block is just in contact with the water, the reaction of water is similar to that of $D = 0.21$ m. Part of the water in contact with the block depresses slightly, but the area with significantly increased pressure under the lower right part of the block is smaller in length and height than that shown in Fig. 8. Under the extrusion of the block, the water under the block is pushed into the right side. In the process of extrusion, the form of water intrusion is longer and narrower. As the block continues to move downward, the water on the right side also reverses under impact. Through comparison, it can be seen that when the water is shallower, the turnover degree of the water is larger and the cavity that forms in the water is smaller. After the collision

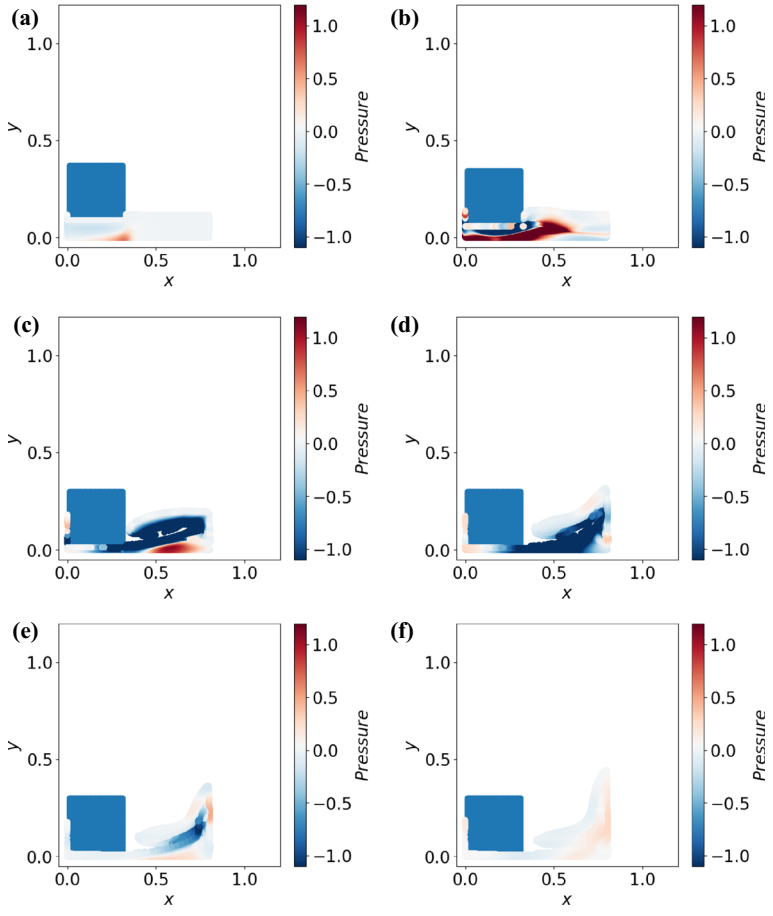

Fig. 7 The surge morphology and pressure distribution diagram. Water depth $D = 0.116$ m and particle density $n = 200/\text{m}$. Each map corresponds to a different moment. **a** 2 dt. **b** 4 dt. **c** 7 dt. **d** 9 dt. **e** 10 dt. **f** 12 dt

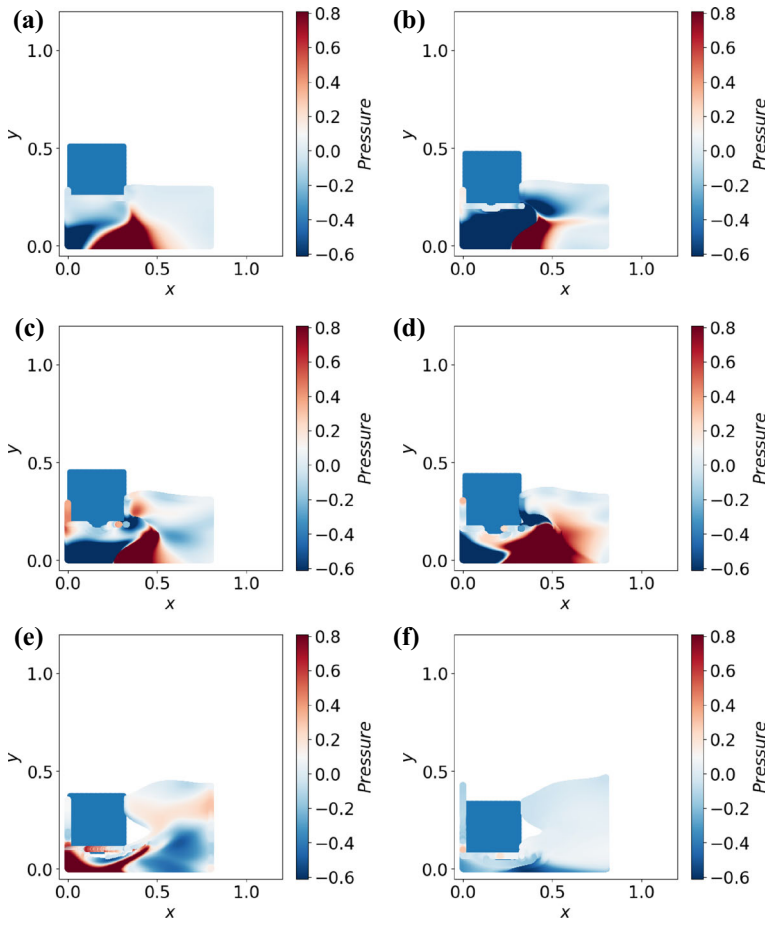

Fig. 8 The surge morphology and pressure distribution diagram. Water depth $D = 0.288$ m and particle density $n = 200/\text{m}$. Each map corresponds to a different moment. **a** 3 dt. **b** 5 dt. **c** 6 dt. **d** 7 dt. **e** 10 dt. **f** 12 dt

with the right wall, part of the water moves upward along the wall, and the other part flows back to the block along the bottom of the tank. Similarly, during the movement, part of the water enters the gap between the block and the left wall and moves upward. But the water in the gap does not exceed the top of the block when the water is shallower.

Simulation results when water depth $D = 0.288$ m

When the water depth increases, the propagation process of the surge also changes to some extent. Figure 8 shows the morphology and pressure changes of the surge at different times when water depth $D = 0.288$ m and particle density $n = 200/\text{m}$. Compared with the simulation results of water depth $D = 0.116$ m and $D = 0.21$ m, the uplift amplitude and morphological changes of water surface are less obvious when the block begins to contact with water due to the large original depth of water. As the block falls into the water, most of the water at the bottom moves to the right under compression, and a small part of the water enters the gap between the block and the left wall and moves upward. The distribution of the area where the water pressure increases significantly under impact and extrusion is similar to the previous results. When the block moves to a certain extent, the water will also turn over, but its turning degree is lower than that when the water is shallower.

Influence of particle density on characteristics of the surge

Simulation results when particle density n = 100/m

Under the condition of the same water depth, different particle densities may also cause differences in surge shape and pressure distribution. Taking water depth $D = 0.21$ m as an example, we analyze the influence of particle density on the propagation process of the surge by changing the particle density. Figure 9 shows the morphology and pressure distribution of the surge at different times when particle density $n = 100/\text{m}$. Compared with Fig. 5, we can see that there are obvious differences in the form and propagation process of the surge. When the block is just in contact with water, the surface of the block has a certain depression. However, the area with high pressure on the lower right of the block is reduced. After the block falls into the water at a certain depth, although the water also moves to the right under the pressure, the uplift amplitude of the water surface is lower than that when particle density n = 200/m. The shape change of the water surface on the right side is not obvious, and the height of particles rising in the left void also decreases.

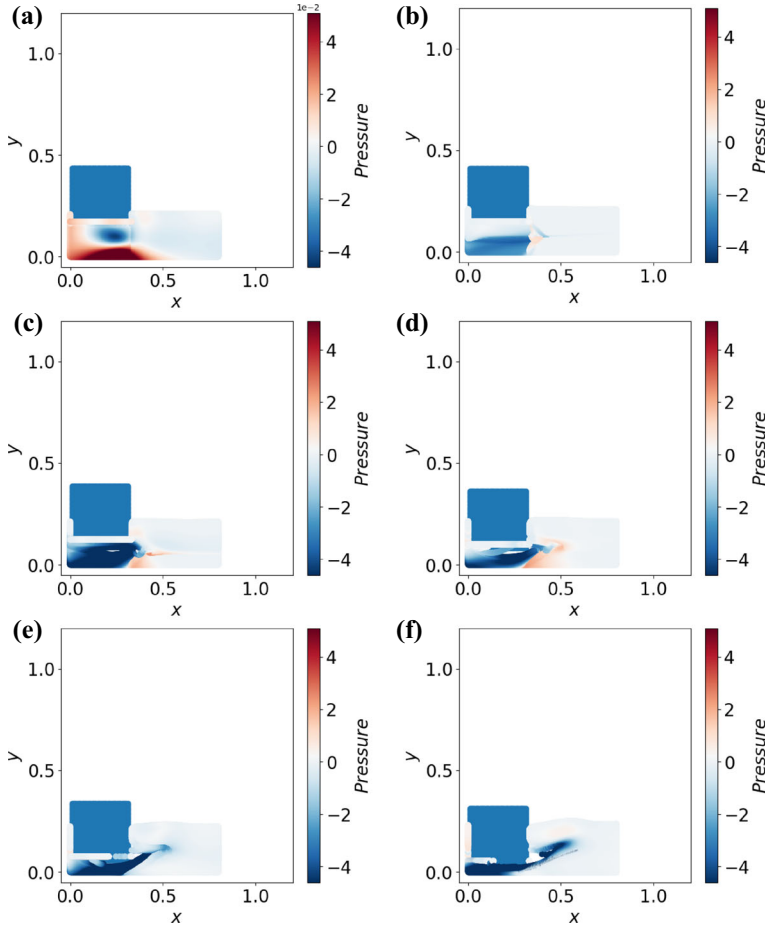

Fig. 9 The surge morphology and pressure distribution diagram. Water depth $D = 0.21$ m and particle density $n = 100/\text{m}$. Each map corresponds to a different moment. **a** 2 dt. **b** 3 dt. **c** 4 dt. **d** 5 dt. **e** 6 dt. **f** 7 dt

Simulation results when particle density n = 300/m

Figure 10 shows the surge morphology and pressure distribution at different times when water depth $D = 0.21$ m and particle density $n = 300/\text{m}$. Compared with Fig. 5, the range and pressure values of the area with higher pressure under the lower right side of the block increase to some extent when the block just making contact with water. At a certain depth, most of the water moves to the right with impact. The uplift amplitude and morphology change of the water surface are similar to the simulation results when the particle density $n = 200/\text{m}$, but the volume of the internal cavity formed when the surge rolls over is smaller.

Discussion

In this paper, we use the PINN to simulate the propagation process of landslide surges. In previous studies, the research area of landslide surges can be roughly divided into the upstream, production area, and downstream. The waves are significantly different in different areas. The first surge occurs when the slide hits the water. When the width of the channel is within a certain range, with the first surge climbing and falling on the opposite bank, the secondary surges generate and spread in the generation area and the

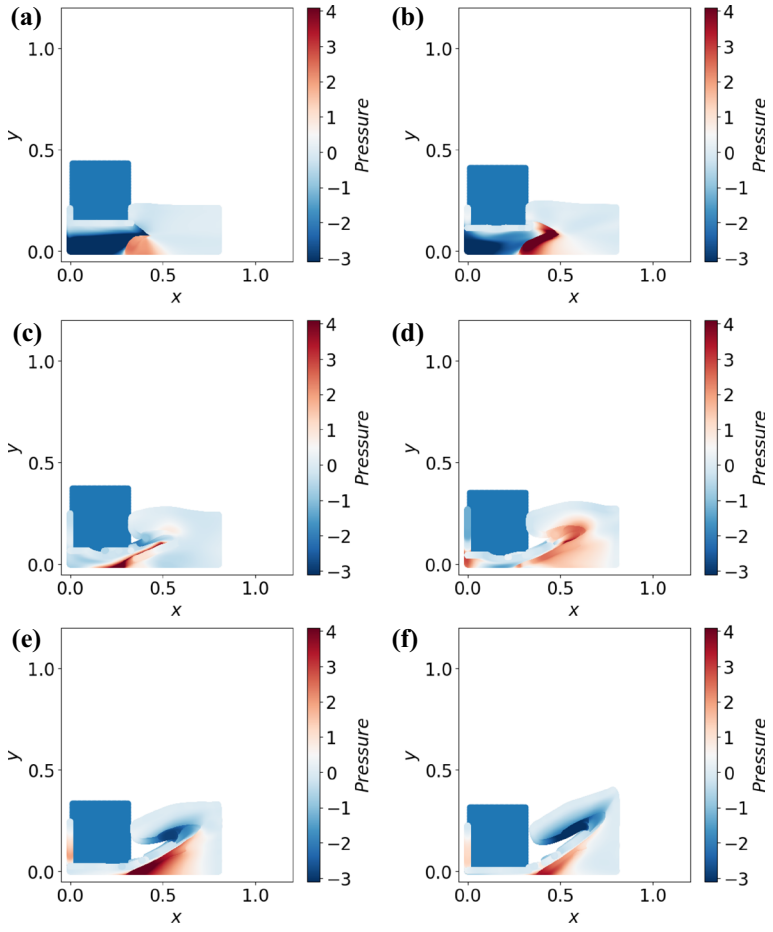

Fig. 10 The surge morphology and pressure distribution diagram. Water depth $D = 0.21$ m and particle density $n = 300/\text{m}$. Each map corresponds to a different moment. **a** 3 dt. **b** 4 dt. **c** 6 dt. **d** 7 dt. **e** 8 dt. **f** 9 dt

transition boundary between the upstream and downstream areas. They are much smaller than the first surge and have a weak influence on the upstream and downstream areas. The generation area gradually becomes calm. The energy of the first surge is largely consumed in the climb to the opposite bank, but cannot be fully transmitted upstream and downstream. The surge height that can be transmitted upstream and downstream is significantly smaller than the first wave height generated by landslide impact. The landslide position has an obvious influence on the damage of the surges [29].

PINN has unique advantages in situations of limited training data, clear initial conditions and boundary conditions, and known related physical laws. Compared with traditional machine learning algorithms, PINN can effectively make use of known physical laws, train models that automatically meet corresponding constraints, and predict important physical parameters of the model by solving inverse problems. Therefore, it is feasible to use PINN to simulate and analyze the movement of landslide surges. However, there are some limitations in using PINN to simulate landslide surges. Generally, PINN is designed according to specific problems. Under different engineering geological conditions, landslide surges may have great differences in morphology and pressure distribution during propagation, which results in that the landslide surge model constructed for a specific case cannot be directly extended to the study of more complex problems. In addition, the choice of network architecture in PINN often has a great influence on the accuracy of the results. In order to get better results, it is usually necessary to make repeated adjustments to get the right network architecture. Moreover, the operation process of PINN is relatively complex, and the training efficiency is greatly affected. Besides, the current PINN is aimed at solving PDE modeling problems. We don't know whether it can be extended to problems without PDE modeling. Therefore, the results of PINN require more specific analysis to further assess their validity. PINN is still in the preliminary stage and there are a lot of problems to solve.

In addition to the PINN used in this paper, many other methods can be applied to the simulation and study of landslide surges and other engineering geological problems. Vacondio et al. [30] firstly applied a three-dimensional Smoothed Particle Hydrodynamics (SPH) model to the falling slide movement and the wave simulation based on the landslide surges generated in Vajont. Rauter et al. [31] proposed a new three-dimensional particle landslide and tsunami model and applied it to some true cases. All these methods may be applied to the simulation and study of landslide surges. In the future, further discussion and analysis will be carried out to obtain more reasonable research results and provide new solutions for the analysis and prediction of geological conditions of large projects such as reservoirs and dams.

The model used in this study still needs some improvement. For example, the model simplifies the landslide to a rigid slide block falling vertically, regardless of the viscosity and compressibility of water and the failure or disintegration process of rock and soil mass. In practical engineering problems, the existence of air will also affect the propagation process of landslide surges. These simplified operations make the model different from the actual situation in simulating landslide surge propagation. In the follow-up study, we will further consider the influence of various factors on the landslide surge propagation process to improve the model and optimize the simulation results.

Conclusions

In this paper, we have a preliminary study on the propagation process of landslide surges using PINN. We simulate and analyze the wave propagation caused by a slide block falling into the water. We have found that: (1) the landslide surge propagation process simulation method based on the physics-informed neural network can well simulate the following stages of landslide surge propagations: a. the local water pressure increases under the extrusion of the slide block, b. the water under the slide block moves to both sides, c. water on both sides of the slide block is uplifted under the impact, d. water overturns and forms cavities inside under extrusion and impact; (2) the depth of water influences the landslide surge propagation as the amplitude of the surge increases with deeper water; (3) the particle density of water influences the landslide surge propagation as the fluctuation of the surge is more obvious with larger particle density. Our research results are of great significance to the study of complex problems related to landslide surges and some similar kinds of problems.

Abbreviations

PINN Physics-informed neural network
DEM Discrete Element Method
DDA Discontinuous Deformation Analysis
NMM Numerical Manifold Method
CFD Computational Fluid Dynamics
SPH Smoothed Particle Hydrodynamics
PDE Partial differential equation
FDM Finite Difference Method
FEM Finite Element Method

Acknowledgements

The authors would like to thank the editor and the reviewers for their constructive reviews of the manuscript and for helpful comments.

Author contributions

All the authors participated in the definition of techniques and algorithms. All authors read and approved the final manuscript.

Funding

This has been funded by the Natural Science Foundation of China (Grant No. 11602235).

Declarations

Availability of data and materials

Not applicable

Competing interests

The authors declare that they have no competing interests.

Received: 31 March 2022 Accepted: 28 June 2022
Published online: 12 July 2022

References

1. Heller V, Hager WH, Minor H-E. Landslide generated impulse waves in reservoirs: Basics and computation. Mitteilungen der Versuchsanstalt fur Wasserbau, Hydrologie und Glaziologie an der Eidgenossischen Technischen Hochschule Zurich. 2009;211:1–172. https://doi.org/10.3929/ethz-b-000157446.
2. Akgün A. Assessment of possible damaged areas due to landslide-induced waves at a constructed reservoir using empirical approaches: Kurtun (North Turkey) dam reservoir area. Nat Hazards Earth Syst Sci. 2011;11(5):1341–50. https://doi.org/10.5194/nhess-11-1341-2011.
3. Fritz HM, Hager WH, Minor H-E. Lituya Bay case: rockslide impact and wave run-up. Sci Tsunami Hazards. 2001;19(1):3–22.
4. Miller DJ. Giant waves in Lituya Bay, Alaska. Bull Seismol Soc Am. 1960;50:253–66. https://doi.org/10.3133/pp354C.
5. Barla G, The Paronuzzi P. Vajont landslide: 50th anniversary. Rock Mech Rock Eng. 1963;2013. https://doi.org/10.1007/s00603-013-0483-7.
6. Heller V, Hager WH. Wave types of landslide generated impulse waves. Ocean Eng. 2011;38(4):630–40. https://doi.org/10.1016/j.oceaneng.2010.12.010.

7. Harbitz CB, Glimsdal S, Løvholt F, Kveldsvik V, Pedersen GK, Jensen A. Rockslide tsunamis in complex fjords: from an unstable rock slope at Åkerneset to tsunami risk in western Norway. Coast Eng. 2014;88:101–22. https://doi.org/10.1016/j.coastaleng.2014.02.003.
8. Noda E. Water waves generated by landslides. J Waterw Harb Coast Eng Div. 1970;96(4):835–55.
9. Kim G-B, Cheng W, Sunny RC, Horrillo JJ, McFall BC, Mohammed F, Fritz HM, Beget J, Kowalik Z. Three dimensional landslide generated tsunamis: numerical and physical model comparisons. Landslides. 2020;17(5):1145–61. https://doi.org/10.1007/s10346-019-01308-2.
10. Yavari-Ramshe S, Ataie-Ashtiani B. Numerical modeling of subaerial and submarine landslide-generated tsunami waves-recent advances and future challenges. Landslides. 2016;13(6):1325–68. https://doi.org/10.1007/s10346-016-0734-2.
11. Mulligan RP, Take WA. On the transfer of momentum from a granular landslide to a water wave. Coast Eng. 2017;125:16–22. https://doi.org/10.1016/j.coastaleng.2017.04.001.
12. Heller V, Spinneken J. On the effect of the water body geometry on landslide-tsunamis: physical insight from laboratory tests and 2D to 3D wave parameter transformation. Coast Eng. 2015;104:113–34. https://doi.org/10.1016/j.coastaleng.2015.06.006.
13. Panizzo A, De Girolamo P, Di Risio M, Maistri A, Petaccia A. Great landslide events in Italian artificial reservoirs. Nat Hazards Earth Syst Sci. 2005;5(5):733–40. https://doi.org/10.5194/nhess-5-733-2005.
14. Horrillo J, Wood A, Kim G-B, Parambath A. A simplified 3-D Navier–Stokes numerical model for landslide-tsunami: application to the Gulf of Mexico. J Geophys Res Oceans. 2013;118(12):6934–50. https://doi.org/10.1002/2012jc008689.
15. Shi G-H. Discontinuous deformation analysis: a new numerical model for the statics and dynamics of deformable block structures. Eng Comput. 1992;9(2):157–68. https://doi.org/10.1108/eb023855.
16. Yu X-Y, Xu T, Heap M, Zhou G-L, Baud P. Numerical approach to creep of rock based on the numerical manifold method. Int J Geomech. 2018. https://doi.org/10.1061/(ASCE)GM.1943-5622.0001286.
17. Mao J, Zhao L, Di Y, Liu X, Xu W. A resolved CFD-DEM approach for the simulation of landslides and impulse waves. Comput Methods Appl Mech Eng. 2020. https://doi.org/10.1016/j.cma.2019.112750.
18. Jiang M, Sun C, Crosta GB, Zhang W. A study of submarine steep slope failures triggered by thermal dissociation of methane hydrates using a coupled CFD-DEM approach. Eng Geol. 2015;190:1–16. https://doi.org/10.1016/j.enggeo.2015.02.007.
19. Tan H, Chen S. A hybrid DEM-SPH model for deformable landslide and its generated surge waves. Adv Water Resour. 2017;108:256–76. https://doi.org/10.1016/j.advwatres.2017.07.023.
20. Xiang Z, Peng W, Zhou W, Yao W. Hybrid finite difference with the physics-informed neural network for solving PDE in complex geometries. arXiv preprint. 2022. arXiv:2202.07926.
21. Solin P, Andrs D, Cerveny J, Simko M. PDE-independent adaptive hp-FEM based on hierarchic extension of finite element spaces. J Comput Appl Math. 2010;233(12):3086–94.
22. Raissi M, Perdikaris P, Karniadakis GE. Physics-informed neural networks: a deep learning framework for solving forward and inverse problems involving nonlinear partial differential equations. J Comput Phys. 2019;378:686–707. https://doi.org/10.1016/j.jcp.2018.10.045.
23. Kissas G, Yang Y, Hwuang E, Witschey WR, Detre JA, Perdikaris P. Machine learning in cardiovascular flows modeling: predicting arterial blood pressure from non-invasive 4D flow MRI data using physics-informed neural networks. Comput Methods Appl Mech Eng. 2020;358: 112623. https://doi.org/10.1016/j.cma.2019.112623.
24. Mao Z, Jagtap AD, Karniadakis GE. Physics-informed neural networks for high-speed flows. Comput Methods Appl Mech Eng. 2020;360: 112789. https://doi.org/10.1016/j.cma.2019.112789.
25. Jin X, Cai S, Li H, Karniadakis GE. NSFnets (Navier–Stokes flow nets): physics-informed neural networks for the incompressible Navier–Stokes equations. J Comput Phys. 2021;426: 109951. https://doi.org/10.1016/j.jcp.2020.109951.
26. Russell JS. Report on waves: made to the meetings of the British association in 1842–43; 1845.
27. Monaghan JJ, Kos A. Scott Russell's wave generator. Phys Fluids. 2000;12(3):622–30. https://doi.org/10.1063/1.870269.
28. Morales JL, Nocedal J. Remark on "algorithm 778: L-BFGS-B: Fortran subroutines for large-scale bound constrained optimization". ACM Trans Math Softw (TOMS). 2011;38(1):1–4.
29. Shi CQ, An Y, Yang JX. A SPH based numerical method of landslide induced impulse and its application on Huangtian landslide event. Sci Sin Phys Mech Astron. 2015;10:9. https://doi.org/10.1360/sspma2015-00280.
30. Vacondio R, Mignosa P, Pagani S. 3d SPH numerical simulation of the wave generated by the Vajont rockslide. Adv Water Resour. 2013;59:146–56. https://doi.org/10.1016/j.advwatres.2013.06.009 (**in Chinese**).
31. Rauter M, Viroulet S, Gylfadóttir SS, Fellin W, Løvholt F. Granular porous landslide tsunami modelling—the 2014 Lake Askja flank collapse. Nat Commun. 2022;13(1):1–13. https://doi.org/10.1038/s41467-022-28296-7.

Publisher's Note